Supplementary Information

Outsmarting Superbugs: The Bactericidal Activity of Nanostructured Titanium Surfaces against methicillin- and gentamicin-resistant *Staphylococcus aureus* ATCC 33592

Jason Wandiyanto,[a] Samuel Cheeseman,[b] Vi Khanh Truong,[b,c] Mohammad Al Kobaisi,[a] Chantal Bizet,[d] Saulius Juodkazis,[e] Helmut Thissen,[f] Russell J. Crawford[b] and Elena P. Ivanova[b*]

[a] *School of Science, Faculty of Science, Engineering and Technology, Swinburne University of Technology, Hawthorn 3122 VIC, Australia*

[b] *School of Science, College of Science, Engineering and Health, RMIT University, Melbourne 3000 VIC, Australia*

[c] *ARC Research Hub for Australian Steel Manufacturing, Wollongong 2500 NSW, Australia*

[d] *Institut Pasteur, CRBIP, 25-28 rue du Dr Roux, 75015 Paris, France*

[e] *Centre for Micro-Photonics, Faculty of Science, Engineering and Technology, Swinburne University of Technology, Hawthorn 3122 VIC, Australia*

[f] *CSIRO Manufacturing, Clayton 3168 VIC, Australia*

*Corresponding Author

Prof. Elena Ivanova

Email: elena.ivanova@rmit.edu.au

KEYWORDS: mechano-bactericidal surfaces; titanium; hydrothermal treatment

S1. Physico-chemical characterisation of the titanium surfaces

XPS analysis revealed the presence of Ti, O and C in abundance on both the AR-Ti and HTE-Ti surfaces, with elemental composition of the surfaces not found to be significantly different (Fig. S1). However, trace quantities of potassium were found on the HTE-Ti surfaces. This is presumed to originate from the KOH during the hydrothermal treatment process [1]. X-ray diffractograms showed no clear difference between the crystalline phases of the AR-Ti and HTE-Ti surfaces (Fig. S2). However, enhanced formation of crystalline titanium dioxide was observed on the HTE-Ti, with an increased ratio between 2Θ peaks of the anatase phase of titanium dioxide (38°) and the alpha phase of titanium (40°).

Surface elemental analysis of AR-Ti and HTE-Ti samples indicate that the AR-Ti is oxidised on the surface which shows both elemental and titanium oxide while only oxidised 6titanium can be seen on the HTE-Ti surface [2-4]. The majority of oxygen is expected to originate from stable titanium oxide (TiO_2), known as Titania. High-resolution XPS-spectra of Ti 2p revealed three peaks (Fig.S1) [2, 3]. Among those, the dominant doublet peaks Ti $2p_{3/2}$ (BE = 459.0 eV) and Ti $2p_{1/2}$ (BE = 464.0 eV) can be unequivocally attributed to TiO_2 [2, 4]. The third, lowest energy peak, is attributable to metallic Ti, with BE = 453 eV for Ti $2p_{3/2}$. The presence of the potassium at high elemental ratio, as seen in Fig. S1B is an evidence that a large percentage of the titanium on the surface is in the form of potassium titanate, which is a result of the basic KOH treatment.

XPS analysis confirmed the presence of Ti, O and C in abundance on both the AR-Ti and HTE-Ti surfaces, with the elemental composition between the surfaces not significantly different (Fig. S1). However, trace quantities of potassium were found on the HTE-Ti surfaces. This is presumed to be remnants of the KOH during the hydrothermal treatment process (Table

S1) [2]. X-ray diffractograms showed no clear difference between the crystalline phases of the AR-Ti and HTE-Ti surfaces (Fig. S1). However, enhanced formation of crystalline titanium dioxide was observed on the HTE-Ti, with an increased ratio between 2Θ peaks of the anatase phase of titanium dioxide (38°) and the alpha phase of titanium (40°). Further details can be found in Fig S1 and Table S1.

High-resolution SEM and AFM imaging demonstrated a densely homogenous coverage of hierarchical sheet-like nanofeatures on the surface of the HTE-Ti which are absent on the AR-Ti surface (Fig. S2). AFM scans displayed an increase of surface roughness (S_a) on HTE-Ti from AR-Ti with values of 26.5 ± 3.8 and 6.2 ± 2.5 respectively. However, the surface roughness between the two samples at the microscale is relatively similar, as seen in Fig. S2B.

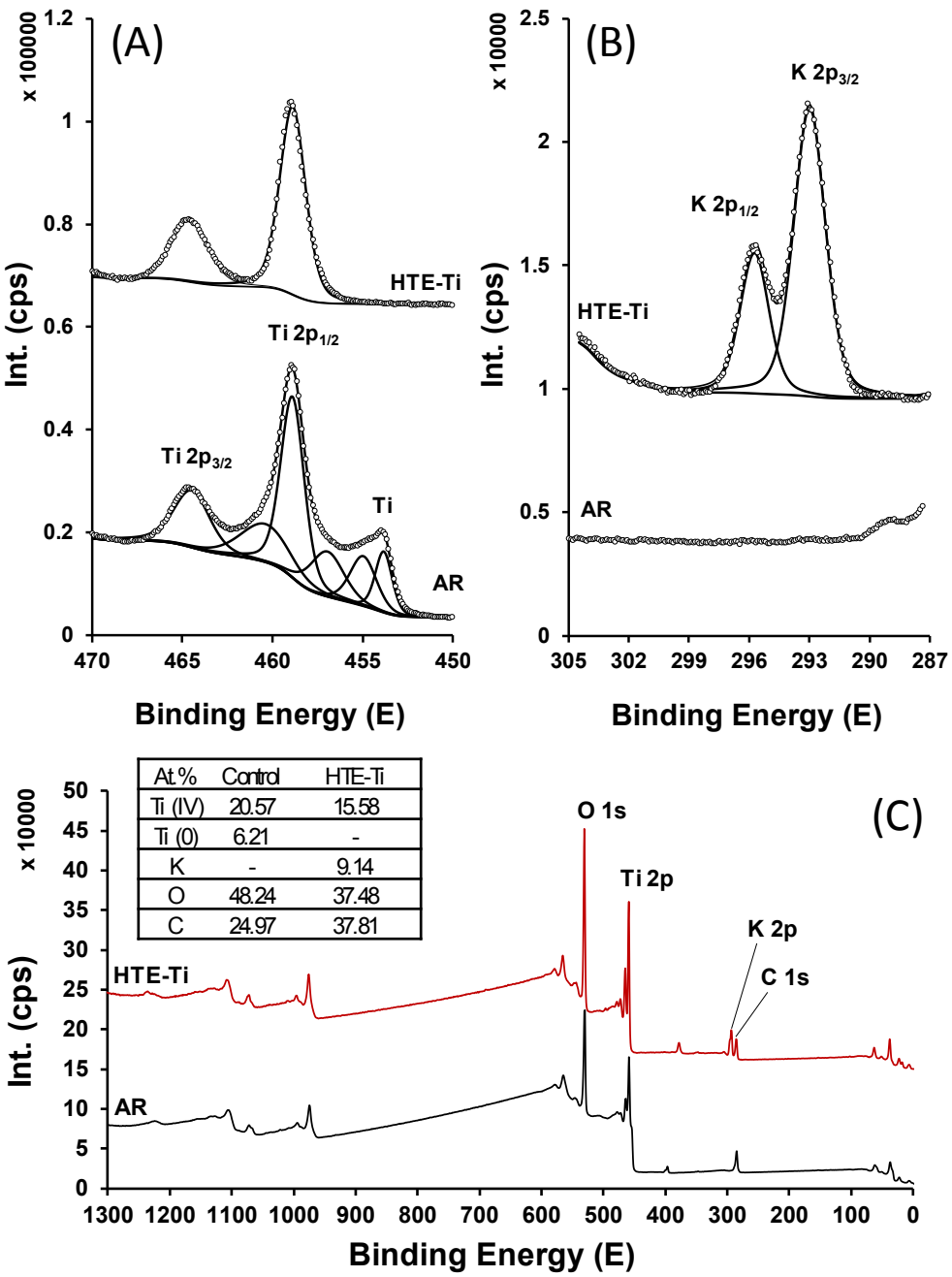

Fig. S1. Elemental analysis of the as-received (AR) and hydrothermally treated (HTE-Ti) titanium surfaces. (A) High-resolution XPS spectra of Ti 2p demonstrating the AR polished metallic and hydrothermally treated oxidised titanium TiO_2. (B) The presence of potassium on the HTE-Ti surface is shown in high-resolution XPS spectra as a result of the hydrothermal treatment. (C) XPS survey spectra of the AR-Ti and HTE-Ti surfaces with Ti 2p, K 2p, and O1s indicated.

X-ray diffractograms demonstrated no clear difference between the crystalline phases of the AR-Ti and HTE-Ti; however, an enhanced formation of crystalline titanium dioxide on the HTE-Ti was noted, with an increased ratio being observed between the 2θ peaks of the anatase phase of titanium dioxide (38°) and the alpha phase of titanium (40°) (Fig. S2). An advantage of using a hydrothermal etching technique is that the surface morphology can be readily controlled by adjusting the parameters of the etching process, which can be performed without significantly changing the surface chemistry or crystallinity [5, 6].

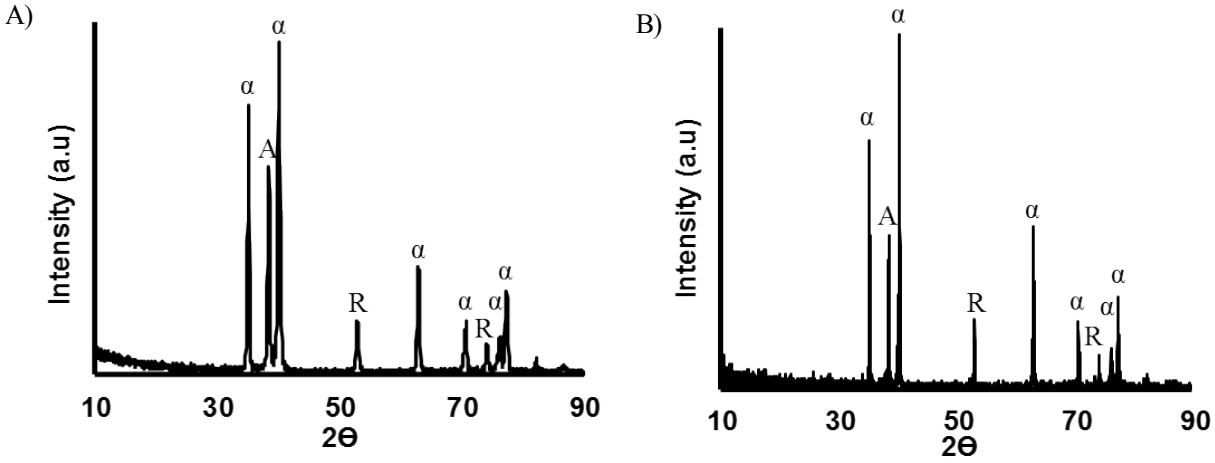

Fig. S2. X-ray diffractogram spectra demonstrating the crystalline phases being present on the AR-Ti (A) and HTE-Ti (B) discs.

Water contact angle measurements revealed that the HTE-Ti surface was more hydrophilic compared to the AR-Ti surface, exhibiting water contact angles of 23.1° ± 4.3° and 58.9° ± 4.8°, respectively (Table S1). This difference can be attributed to the trace amount of potassium on the HTE-Ti surface [1, 2, 7].

S2. Surface topography of the HTE-Ti and AR-Ti surfaces

High-resolution SEM and AFM imaging demonstrated a densely homogenous coverage of hierarchical sheet-like nanofeatures on the surface of the HTE-Ti, which are not present on the AR-Ti surface (Fig. S3). It should be noted that the microscale topography of the HTE-Ti is relatively similar to the AR-Ti surface (Fig. S3B). HTE-Ti surface exhibited higher average S_a and S_q values of 26.5 ± 3.77 nm and 33.87 ± 5.60 nm, respectively, while AR-Ti surfaces of S_a = 6.23 ± 2.47 nm and S_q = 8.84 ± 2.47 nm, respectively.

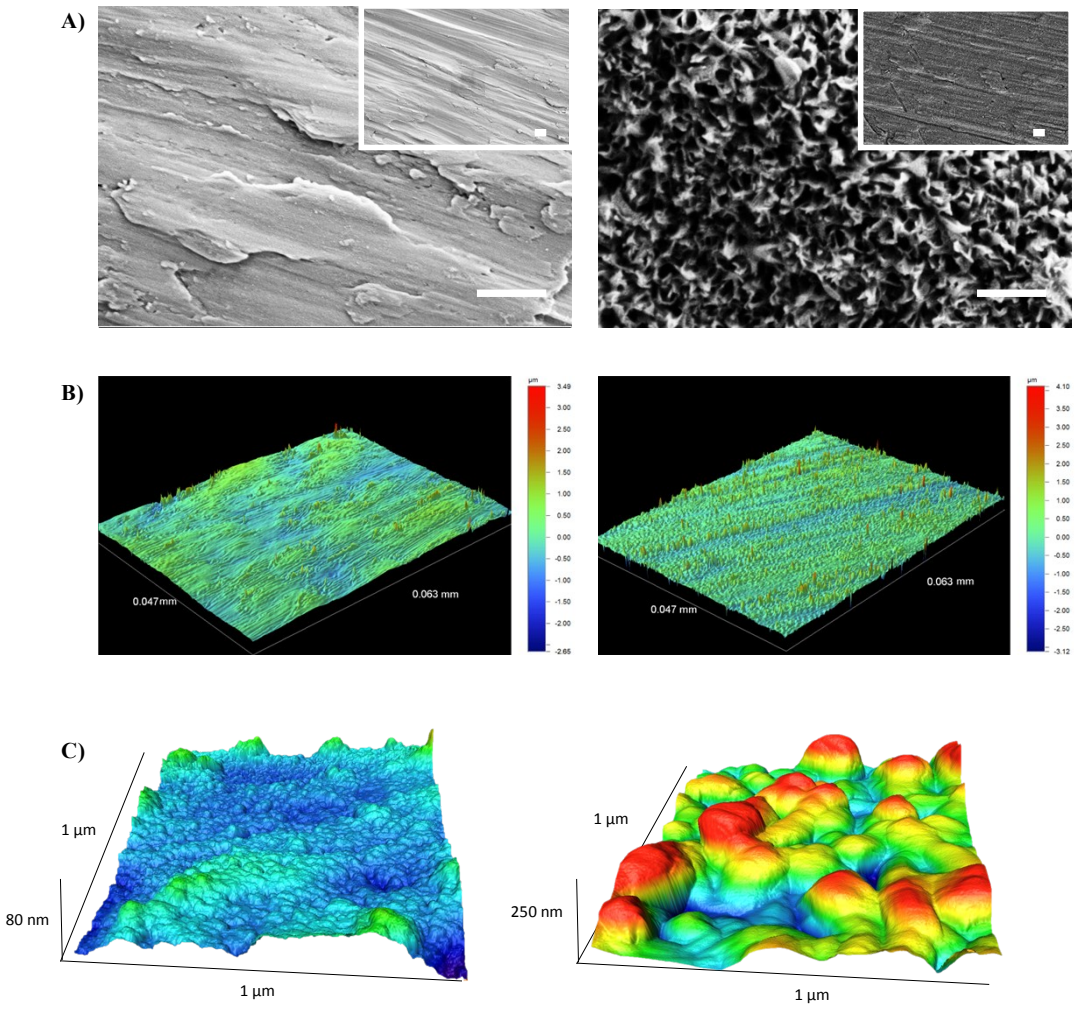

Fig. S3. Topographical characterisation of AR-Ti (left) and HTE-Ti (right) surfaces. (A) SEM images (scale bar = 400 nm, inset scale bar = 2 µm), (B) 3D optical profilometry images and (C) 3D AFM images of the AR-Ti and HTE-Ti surfaces.

Table S1. Surface topography and wettability of HTE-Ti and AR-Ti surfaces.*

Surface roughness parameters	HTE-Ti	AR-Ti
S_a *(nm)*	6.2 ± 2.5	26.5 ± 3.8
S_q *(nm)*	8.8 ± 3.9	33.9 ± 5.6
S_{sk}	0.1 ± 0.9	-0.2 ± 0.1
S_{ku}	2.5 ± 1.1	0.2 ± 0.1
Water contact angle (degrees)	23.1 ± 4.3	58.9 ± 4.8

*Surface roughness parameters obtained from AFM scans of 1 × 1 μm^2.

S3. Kirby-Bauer susceptibility test

The resistance and susceptibility between the antibiotic-resistant and the antibiotic-susceptible *S. aureus* strains were determined by the Kirby-Bauer disc diffusion method against methicillin and gentamicin (Fig. S5) with minimum inhibitory concentrations of 5 µg/mL and 10 µg/mL being observed respectively. After 18 hour incubation at 37 °C, zones of inhibition were seen on antibiotic-susceptible *S. aureus* around the discs (left), however no zones of inhibition were seen around methicillin- and gentamicin-resistant strain (right), indicating their resistance against the antibiotic.

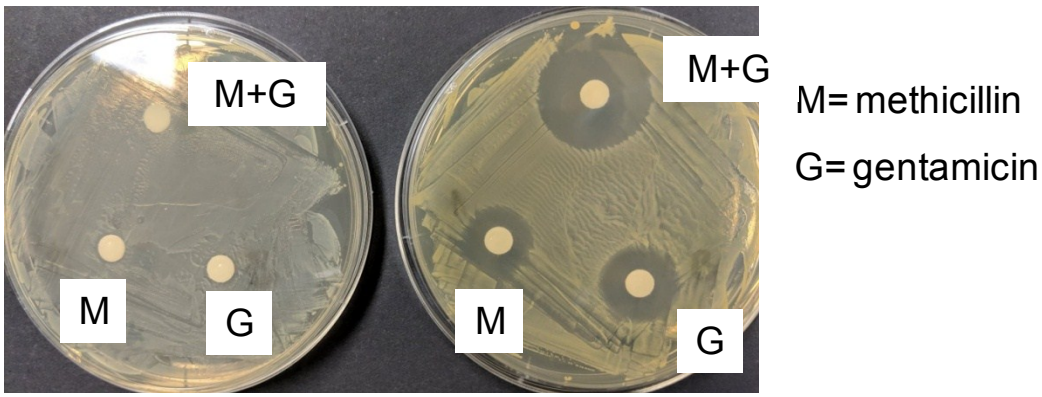

Fig. S4. Antibiotic susceptibility testing. Susceptible *S. aureus* (right) displays a zone of inhibition around methicillin (M), gentamicin (G) and both antibiotics (M+G), where the cells

were unable to grow within the halo, while the methicillin- and gentamicin-resistant *S. aureus* (left) demonstrates complete coverage of the agar plate, indicating resistance.

S4. Antibiotic susceptibility of the *S. aureus* CIP 65.8^{T} (MSSA) and *S. aureus* ATCC 33592 (MRSA)

Mechanism of methicillin resistance in *S. aureus*

Methicillin-resistant *S. aureus* strains are thought to have emerged through the acquisition of the staphylococcal cassette chromosome *mec* (SCC*mec*), facilitating expression of the PBP conjugate protein PBP2A, which, unlike PBP, does not interact with methicillin [8, 9]. SCC*mec* codes for three types of proteins [8-10]. The *mecl* gene encodes a repressor protein, *mecR1* encodes a signal-transduction protein and *mecA* encodes for PBP2A. PBP2A does not bind to the beta-lactam structure and in the presence of methicillin takes over the role of PBP; cross-linking the layers of peptidoglycan in the cell wall [9, 10]. In the presence of methicillin, MecR1 senses the presence of β-lactam antibiotics and activates a cytoplasmic domain, as a protease, through autocatalytic cleavage [8]. It then cleaves the Mecl repressor protein, which is bound to the *mecA* gene, enabling transcription of *mecA*, resulting in the expression of PBP2A [8, 9, 11]. Although a conjugate of PBP, PBP2A is considered a poorer transpeptidase, resulting in the formation of peptidoglycan layers of a lower quality [12, 13].

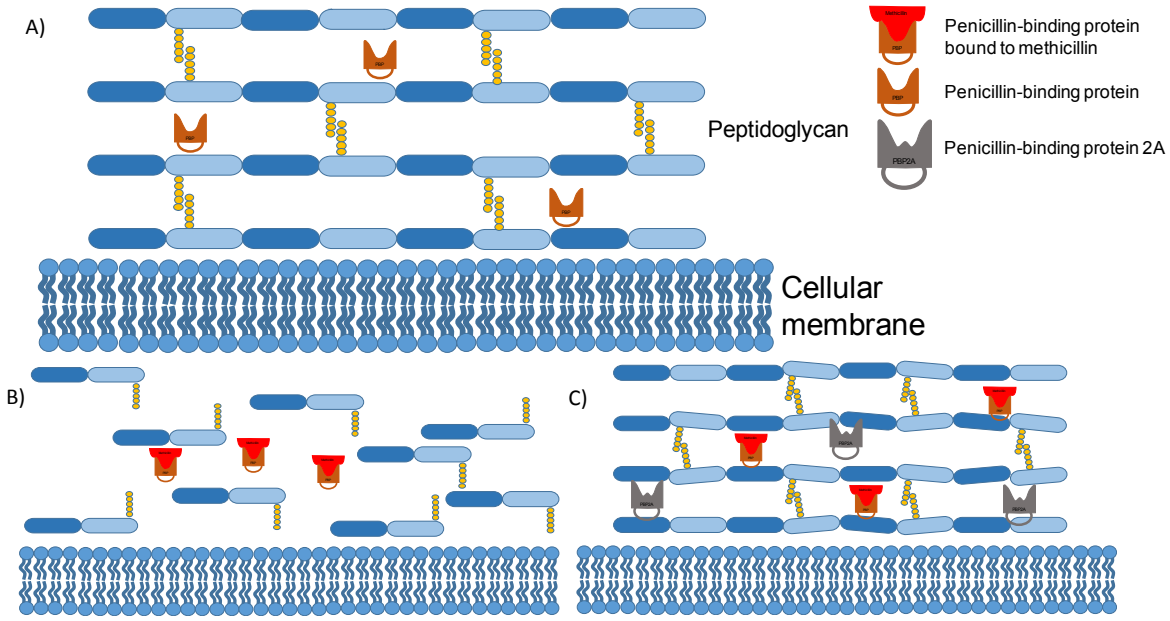

Fig. S5. A schematic of the cell membrane of *S. aureus*. A) In the absence of methicillin, the cell wall contains the cellular membrane and layers of peptidoglycan. B) In the presence of methicillin, the antibiotic binds to the penicillin-binding protein (PBP) which is responsible for cross-linking the peptidoglycan layers in the cell walls. The resulting cell wall of methicillin-susceptible *S. aureus* strains lacks complete peptidoglycan layers. C) Inside the methicillin-resistant *S. aureus* strain, the cells express PBP2A, a conjugate protein of PBP, which does a partial job of PBP and has a lower affinity towards methicillin compared to PBP. Therefore, the methicillin-resistant strain can still synthesize the peptidoglycan cell wall in the presence of methicillin, however, the peptidoglycan cell wall synthesized in the presence of methicillin is different from the peptidoglycan cell wall synthesized in the absence of methicillin.

S5. Investigating the influence of methicillin and gentamicin on the attachment of methicillin-susceptible *S. aureus*

To further, understand the effects of the antibiotics on the attachment propensity of methicillin-susceptible *S. aureus*, the attachment was studied on as received silicon and glass surfaces, for comparison with the Ti surfaces. The bacteria were incubated on the surfaces in the presence of methicillin and gentamicin for 18 h as described in section 2.4. For comparison,

some cells were inactivated by heat treatment and incubated on the surface in the absence of the antibiotics for 18 h. To inactivate *S. aureus* by heat, a stock solution of the bacteria was heated to 80 °C for 20 minutes, as described [14]. The cell density was then adjusted to OD_{600} = 0.1 and added to the samples as described in methods; section 2.5.

Confocal laser scanning micrographs demonstrated a significant increase in attachment from the heat-treated methicillin-susceptible *S. aureus* compared to the susceptible *S. aureus* incubated in the presence of the antibiotics (Fig. S6). However, the bacterial interaction with different material such as silicon wafer and glass was different as shown in Fig S6. It is likely the observed difference in bacterial attachment between the two treatments is due to the composition of the bacterial cell wall. Methicillin disrupts the proper formation of the protective layers of peptidoglycan, which may affect the cell surface properties and reduce the propensity of attachment. Conversely, the heat-treated cells likely possess a cell wall composition similar to untreated, control cells.

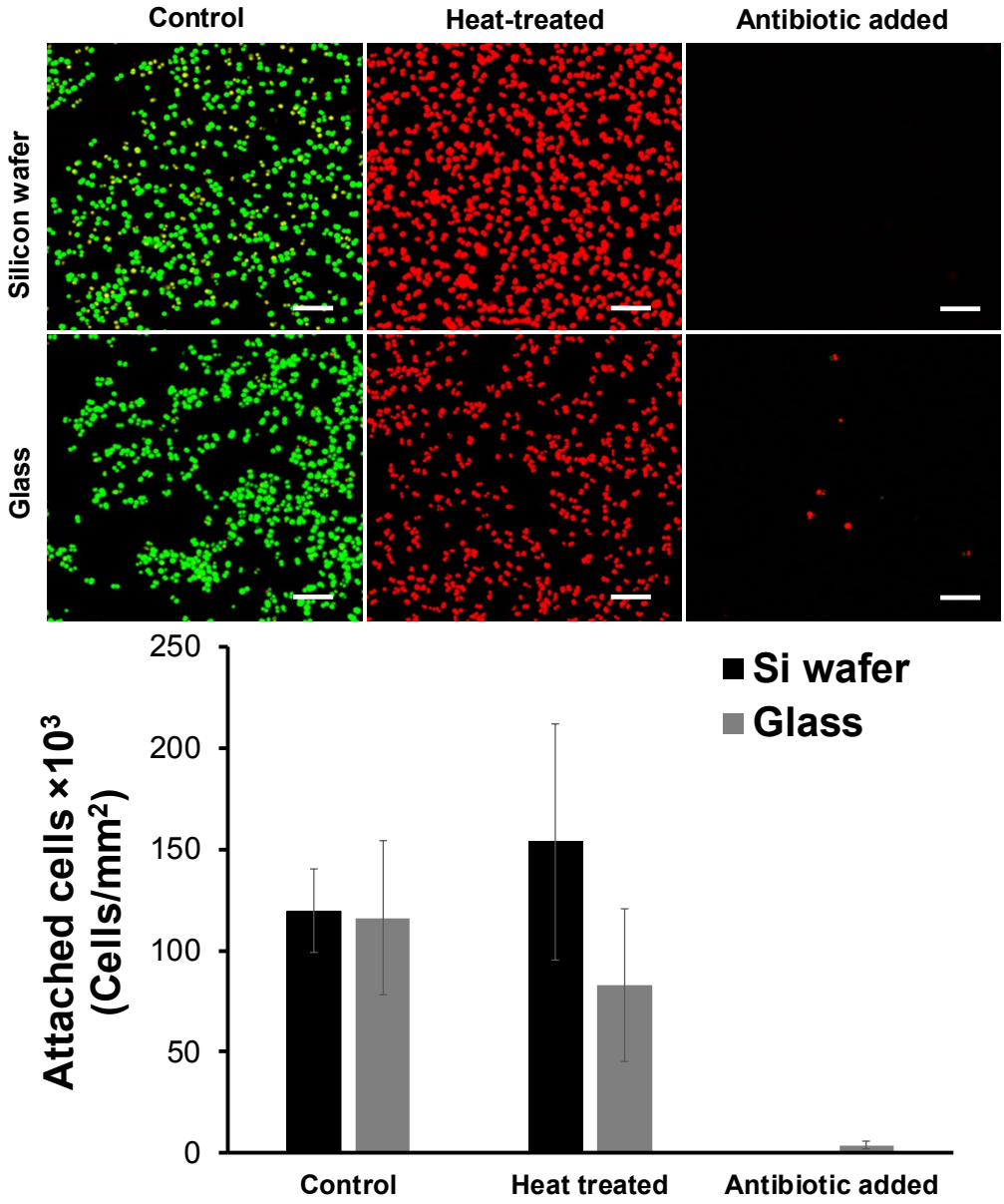

Fig S6. The difference in attachment propensity of intact, heat inactivated and in the presence of antibiotics of methicillin-susceptible *S. aureus* on silicon and glass surfaces after 18 h incubation. (Top) CLSM images demonstrating the viability of bacterial cells. (Bottom) The attachment density of the methicillin-susceptible *S. aureus*.

References

[1] S. Mei, H. Wang, W. Wang, L. Tong, H. Pan, C. Ruan, Q. Ma, M. Liu, H. Yang, L. Zhang, Y. Cheng, Y. Zhang, L. Zhao, P.K. Chu, Antibacterial effects and biocompatibility of titanium surfaces with graded silver incorporation in titania nanotubes, Biomaterials 35(14) (2014) 4255-4265.

[2] C.M. Bhadra, V. Khanh Truong, V.T.H. Pham, M. Al Kobaisi, G. Seniutinas, J.Y. Wang, S. Juodkazis, R.J. Crawford, E.P. Ivanova, Antibacterial titanium nano-patterned arrays inspired by dragonfly wings, Sci. Rep. 5 (2015) 16817.

[3] V.K. Truong, S. Rundell, R. Lapovok, Y. Estrin, J.Y. Wang, C.C. Berndt, D.G. Barnes, C.J. Fluke, R.J. Crawford, E.P. Ivanova, Effect of ultrafine-grained titanium surfaces on adhesion of bacteria, Applied Microbiology and Biotechnology 83(5) (2009) 925-937.

[4] S.A. Pawar, R.S. Devan, D.S. Patil, V.V. Burungale, T.S. Bhat, S.S. Mali, S.W. Shin, J.E. Ae, C.K. Hong, Y.R. Ma, J.H. Kim, P.S. Patil, Hydrothermal growth of photoelectrochemically active titanium dioxide cauliflower-like nanostructures, Electrochimica Acta 117 (2014) 470-479.

[5] K. Zhu, G. Hu, Supercritical hydrothermal synthesis of titanium dioxide nanostructures with controlled phase and morphology, Journal of Supercritical Fluids 94 (2014) 165-173.

[6] T.H.T. Vu, H.T. Au, L.T. Tran, T.M.T. Nguyen, T.T.T. Tran, M.T. Pham, M.H. Do, D.L. Nguyen, Synthesis of titanium dioxide nanotubes via one-step dynamic hydrothermal process, Journal of Materials Science 49(16) (2014) 5617-5625.

[7] P.M. Tsimbouri, L. Fisher, N. Holloway, T. Sjostrom, A.H. Nobbs, R.M.D. Meek, B. Su, M.J. Dalby, Osteogenic and bactericidal surfaces from hydrothermal titania nanowires on titanium substrates, Sci. Rep. 6 (2016).

[8] K. Hiramatsu, L. Cui, M. Kuroda, T. Ito, The emergence and evolution of methicillin-resistant *Staphylococcus aureus*, Trends Microbiol. 9(10) (2001) 486-493.

[9] P.D. Stapleton, P.W. Taylor, Methicillin resistance in *Staphylococcus aureus*: mechanisms and modulation, Sci. Prog. 85(1) (2002) 57-72.

[10] A.L. Lovering, M.C. Gretes, S.S. Safadi, F. Danel, L. de Castro, M.G.P. Page, N.C.J. Strynadka, Structural insights into the anti-methicillin-resistant *Staphylococcus aureus* (MRSA) activity of ceftobiprole, J. Biol. Chem. 287(38) (2012) 32096.

[11] B.J. Wilkinson, K.J. Dorian, L.D. Sabath, Cell wall composition and associated properties of methicillin-resistant *Staphylococcus aureus* strains, J. Bacteriol. 136(3) (1978) 976-982.

[12] M. Haenle, A. Fritsche, C. Zietz, R. Bader, F. Heidenau, W. Mittelmeier, H. Gollwitzer, An extended spectrum bactericidal titanium dioxide (TiO2) coating for metallic implants: In vitro effectiveness against MRSA and mechanical properties, J. Mater. Sci.: Mater. Med. 22(2) (2011) 381-387.

[13] R. Benveniste, J. Davies, Mechanisms of antibiotic resistance in bacteria, Annu. Rev. Biochem. 42(1) (1973) 471-506.

[14] M.N. Yaniarti, C. Amarantini, T.Y. Budiarso, The effect of temperature and Pasteurization time on *Staphylococcus aureus* isolates from dairy products, AIP Conference Proceedings, American Institute of Physics, 2017, p. 050003.